Journal of Industrial and Engineering Chemistry 80 (2019) 686–695

Contents lists available at ScienceDirect

Journal of Industrial and Engineering Chemistry

journal homepage: www.elsevier.com/locate/jiec

Efficient bifunctional catalytic activity of nanoscopic Pd-decorated $La_{0.6}Sr_{0.4}CoO_{3-\delta}$ perovskite toward Li–O_2 battery, oxygen reduction, and oxygen evolution reactions

Mi Young Oh[a], Jong Ju Lee[b], Hyo Seok Park[b], Tae-Young Kim[d], Yun-Sung Lee[e,*], Vanchiappan Aravindan[f], Kee Suk Nahm[a,b,c,**]

[a] R&D Education Center for Fuel Cell Materials & Systems, Jeonju 561-756, Republic of Korea
[b] Department of Energy Storage and Conversion Engineering, Jeonju 561-756, Republic of Korea
[c] School of Chemical Engineering, Chonbuk National University, Jeonju 561-756, Republic of Korea
[d] Buan Fuel Cell Center, Korea Institute of Energy Research (KIER), Jellabuk-do 56332, Republic of Korea
[e] School of Chemical Engineering, Chonnam National University, Gwang-ju 61186, Republic of Korea
[f] Department of Chemistry, Indian Institute of Science Education and Research (IISER), Tirupati, 517507, India

ARTICLE INFO

Article history:
Received 24 April 2019
Received in revised form 14 August 2019
Accepted 20 August 2019
Available online 24 August 2019

Keywords:
Perovskite oxide
Pd decoration
Catalytic activities
Lithium-oxygen battery
Electrocatalyst

ABSTRACT

Palladium decoration is performed on $La_{0.6}Sr_{0.4}CoO_{3-\delta}$ (LSC) with different loadings (5 to 30 wt.%) to improve its oxygen reduction reaction (ORR) activity without sacrificing its oxygen evolution reaction (OER) capability. The Pd decoration yields a higher specific surface area as loading concentration increases and leads to the formation of more porous active sites for efficient activity. Both aqueous and organic media are used to study the electrocatalytic activity of the prepared Pd-LSC composite. In aqueous media, the Pd-LSC materials exhibit higher ORR and OER activities than native LSC and RuO_2. For example, as Pd loading increases in aqueous media ($5 < 10 < 20 < 30$ wt.%), the performance improves and becomes comparable to the that of a conventional Pt/C catalyst, whereas 20 wt.% loading establishes better OER activity. This interesting result in aqueous media logically alerts us to study the electrocatalytic activity in organic medium toward Li-O_2 battery application. Similar to the aqueous media, the Pd-LSC composite outperformed the native materials, like LSC and ketjen black. More specifically, 30 wt.% loading delivers the highest discharge capacity and longest cycle life compared to the other compositions. Postmortem studies are also performed to ensure the electrocatalytic activity of the Pd-LSC composite.

Introduction

Li-O_2 batteries are considered strong contenders for electric vehicle applications owing to the higher gravimetric energy density (12 kW h kg^{-1}) than conventional gasoline (13 kW h kg^{-1}) systems. Further, the energy density of a Li-O_2 battery is ~10 times more than that of present Li-ion batteries [1–7]. Unfortunately, the Li-O_2 chemistry limits its potential for commercial applications, including its lack of reversibility, cell design, large overpotential, poor rate cyclability, and improper choice of catalysts. The poor reaction kinetics associated with the oxygen electrode during the charge–discharge process is also worth noting [8]. Improving the reaction kinetics toward the oxygen electrode is one efficient approach to address many of the aforementioned issues, hence, extensive research has been conducted to utilize the appropriate catalyst. More specifically, the choice and efficient utilization of electrocatalysts for the O_2 electrode, such as transition metal oxides [7], carbonaceous materials [9,10], ultrafine Pt or Pt/C composites [11], binary metal alloys like Pt-Au nanostructures, and perovskites [12,13], have been explored. Although significant advancements and improvements in terms of the oxygen reduction reaction (ORR) and oxygen evolution reaction (OER) are realized, the overall battery performance remains insufficient for real application. This clearly suggests that there is an opportunity to explore efficient bifunctional electrocatalysts to improve the electrochemical performance of such fascinating Li-O_2 configuration.

* Corresponding author.
** Corresponding author at: Department of Energy Storage and Conversion Engineering, Jeonju 561-756, Republic of Korea.
E-mail addresses: leeys@chonnam.ac.kr (Y.-S. Lee), nahmks@jbnu.ac.kr (K.S. Nahm).

https://doi.org/10.1016/j.jiec.2019.08.045
1226-086X/

Perovskites are known for their catalytic activity (OER), particularly in fuel cells due to the favorable physiochemical properties, like high ionic conductivity, and tunable structural properties [12,14–20]. Li-O_2 is considered a semi-fuel cell, in which the use of two different kinds of catalyst for ORR and OER activity is highly challenging in terms of engineering and cell design. Therefore, the exploration of bifunctional catalysts is desperately required to complete the formation and decomposition of Li_2O_2 during the electrochemical reaction. Recently, various perovskites, i.e., Cu nanoparticle-loaded $Sr_{0.95}Ce_{0.05}CoO_{3-\delta}$ [14], $La_{0.5}Sr_{0.5}CoO_{2.91}$ [21], $La_{0.6}Sr_{0.4}CoO_{3-\delta}$ (LSC) [22], and $La_{0.8}Sr_{0.2}MnO_{3-\delta}$ [23], have been extensively investigated as efficient bifunctional catalysts in Li-O_2 batteries. It is worth reporting that $LaNiO_3$ possesses unique intrinsic activity for both ORR and OER corresponding with molecular orbital principle calculations [12,24]. $LaNiO_3$ [25] and its derivatives ($LaNi_{1-x}Mg_xO_3$ (x = 0, 0.08, 0.15) [26], g-C_3N_4-$LaNiO_3$ composites [27]) have also been studied as oxygen cathode catalysts in Li-O_2 batteries. Zhang et al. [25] reported the glycine-assisted preparation of porous $LaNiO_3$ (35.8 $m^2\ g^{-1}$), which was approximately 10 times higher in surface area than pristine $LaNiO_3$. Concerning the Li-O_2 battery efficiency of both materials, the glycine-assisted porous $LaNiO_3$-based cell exhibited much better performance (discharge capacity = 3407 mAh g^{-1} and overpotential = 1.17 V) than $LaNiO_3$ (discharge capacity = 2639 mAh g^{-1} and overpotential = 1.63 V). Unfortunately, the performance of the Li-O_2 cell is far beyond the expectations; for example, Zhao et al. [21] reported the hierarchical mesoporous $La_{0.5}Sr_{0.5}CoO_{2.91}$ nanostructures that exhibit very high discharge capacity, but the small pores present were easily clogged by the discharge product, Li_2O_2, leading to the poor cycling stability by this inferior catalytic behavior. In our previous study, an LSC perovskite was synthesized and employed as an electrocatalyst for an Li-O_2 battery system [28,29]. Apparently, the LSC perovskite exhibited good catalytic activity in OER, much better than commercial Pt/C, RuO_2, and ketjen black (KB), whereas, the ORR activity was found to be inferior compared to the commercial Pt/C. Among the various ORR electrocatalysts, Pd appears to be the better substitute for Pt as they share many similar properties [30]. It is well-established that Pd is an efficient ORR active catalyst for Li-O_2 batteries and fuel-cells, besides the applications like bio-sensing and CO_2 oxidation, among others [31]. Regarding this, we designed a synthesis strategy to prepare an efficient electrocatalyst to promote Li-O_2 cell performance by enhancing the ORR activity through the controlled decoration of Pd over the surface of LSC. Accordingly, four different concentrations of Pd decoration over the LSC surface were performed by the Pechini process. First, the catalytic activity of the Pd-decorated LSCs was studied in aqueous solution and subsequently in an organic medium. Finally, the Pd-decorated LSC catalysts were applied as an air electrode catalyst for a Li-O_2 battery, which will be discussed in detail.

Experimental

Synthesis of $La_{0.6}Sr_{0.4}CoO_{3-\delta}$ (LSC)

The Pechini process was used to synthesize the perovskite LSC. In a typical synthetic protocol, a stoichiometric ratio of La$(NO_3)_3.6H_2O$ (99.9%, Sigma–Aldrich), $Sr(NO_3)_2$ (99%, Sigma–Aldrich), $Co(NO_3)_2.6H_2O$ (97.7%, Sigma–Aldrich) were dissolved separately in deionized (DI) water, and finally mixed together. After mixing the solution, citric acid (99.5%, Sigma–Aldrich) was added to form a metal complex. Then, polymerization was performed by introducing ethylene glycol (99%, Sigma–Aldrich) into the above solution and continuously stirring for 2 h to form the gel. The gel was dried and subsequently carbonized at 400 °C for 1 h to remove organic moieties followed by high-temperature calcination at 1000 °C for 4 h. The detailed optimization procedure of LSC was reported in our previous work [28,29]. Hence, all the synthesis protocol for Pd-decoration over LSC was carried out at 1000 °C.

Pd-deposition on LSC

Palladium (II) nitrate dihydrate ($Pd(NO_3)_2.2H_2O$, Sigma–Aldrich) was used as the Pd precursor. For the loading of 5, 10, 20, and 30 wt.% of Pd on LSC, stoichiometric amounts (0.013, 0.027, 0.062, and 0.107 g, respectively) of Pd $(NO_3)_2{\cdot}2H_2O$ were dissolved in 100 ml DI water and continuously stirred for 30 min to ensure complete dissolution. Then, 0.1 g of LSC was added to the solution and vigorously stirred for 1 h. Highly concentrated (10 mol) sodium borohydride (98.5% $NaBH_4$) solution was added dropwise to the mixed solution to form Pd on the LSC surface by reducing Pd^{2+} in the solution. This process was continued for 2 h to ensure the complete reduction of Pd^{2+}. Then, the products (Pd-LSC) were repeatedly washed with DI water and vacuum dried at 80 °C for 12 h. The same procedure was repeated for all concentrations of Pd.

Structural characterizations

Powder X-ray diffraction (XRD) measurements were performed to study the crystal structures of Pd-LSC with Cu Kα (λ = 1.54059 Å). The surface morphological properties were analyzed with field emission scanning electron microscopy (FE-SEM, JSM–6700F), and corrected scanning transmission electron microscopy (CS–TEM, JEM–ARM200F, JEOL). Brunauer–Emmett–Teller (BET) surface area measurements were conducted using BELSORP-mini II (BEL Japan, Inc., Japan). Inductively coupled plasma mass spectrometry (ICP-MS, Agilent 7500a, and Agilent Technologies) and X-ray photoelectron spectroscopy (XPS, Thermo Scientific) were used to study the bulk and surface chemical compositions, respectively.

Electrochemical studies

Linear sweep voltammetry (LSV) was employed to study the electrocatalytic activities of the synthesized Pd-LSC toward the ORR and OER using CHI700C at room temperature. A three-electrode setup was used in the presence of a mild alkaline solution (0.1 M KOH) as the electrolyte, Pt-wire as the counter electrode, and Hg/HgO as a reference electrode. For the preparation of the working electrode, Pd-LSC was mixed with Vulcan carbon (Cabot Vulcan XC-72) with the weight ratio of 3:7 to provide sufficient electronic conductivity. Approximately 10 mg of the as-prepared mixed powders were dispersed ultrasonically in 150 μL of diluted Nafion alcohol solution (5 wt.%) dissolved in isopropyl alcohol (IPA). An amount of 13.5 μL of the suspension (active material loading: 9.88 μg) was pipetted onto a glassy carbon substrate with an area of 0.25 cm^2. The electrolyte in the cell was enriched with O_2 for 1 h prior to the LSV measurements. The scan rate (5 mV s^{-1}) and disk rotation rate (1600 rpm) were fixed for a rotating ring-disk electrode. KB (EC600JD) and 30 wt.% Pt/C (Premetek Co.) electrodes were also prepared and subjected to the same experimental conditions for comparison.

The ORR and OER performances in the non–aqueous medium were measured using cyclic voltammetry (CV) with Solatron. CV was performed at a scan rate of 0.01 mV s^{-1} between 1.5 and 4.7 V using a Swagelok™ type cell with a Pd-LSC (0.5 mg)-catalyzed air cathode in non-aqueous lithium bis(trifluoromethane)sulfonimide (LiTFSI) in tetraethylene glycol dimethyl ether (TEGDME) electrolyte (210 μL) in which metallic Li served as the counter electrode. The electrolyte used in this experiment was prepared by dissolving 99.95% purity LiTFSI in 99% purity TEGDME without further refining, and was used within a limited period of 3 months to ensure reproducibility of the experimental data. For the Li-O_2

battery setup, the same Swagelok™-type cells were used. A battery tester (BTS 2000W, Japan) was used to record the charge–discharge profiles under oxygen flow (10 cc $min.^{-1}$) at a current density of 0.1 mA cm^{-2} between 2.0 and 4.3 V vs. Li. The working electrode was prepared by mixing the Pd-LSC catalyst and KB (at a ratio of 1:2) with teflonized acetylene black (TAB) binder (60%) in IPA. The resultant mixture was prepared (1 cm diameter) and pressed on a Ni mesh (1.2 cm diameter), and subsequently vacuum dried at 100 °C for 12 h prior to use. To fabricate the Swagelok™-type cell, Li metal foil was used as an anode, glass fiber as a separator, and 1 M LiTFSI in TEGDME as the electrolyte. All battery performance tests were repeated three times to ensure reproducibility with negligible deviation in the results.

Results and discussion

Structural analysis

Fig. 1 represents the XRD patterns of the synthesized Pd-LSC materials with different amounts of Pd loadings (5, 10, 20, and 30 wt.%). Fig. 1a and b represent the characteristic reflections for Pd and LSC, which are consistent with the literature JCPDS No. 46-1043 and JSPDS 36–1393, respectively [13,22]. The synthesized Pd-LSC composites (5, 10, 20, and 30 wt.% Pd) exhibit well-defined diffraction peaks (Figs. 1c–f), which confirm the crystalline nature of the prepared compounds with appropriate synthesis protocol. However, the diffraction peak intensity varies with the increase in Pd loading. As the Pd concentration increases from 5 to 10, 20, and 30 wt.%, the peak intensity of the characteristic reflection of Pd ($2\theta = 39.8°$) gradually increased, while the characteristic doublet peaks gradually decreased ($2\theta = 33°$) for LSC. The decrease in peak intensity is clearly evident from the XRD patterns. This is mainly due to the increase in nanoscopic Pd particle deposition over the LSC surface, which overshadows the intensity of the native compound. The effect of such nanoscopic Pd decoration over LSC with various loadings only occurs on the surface or bulk properties; the lattice parameter values were calculated and compared via the Rietveld analysis is given in Table S1. The measured lattice parameters of the Pd-LSC samples exhibit close proximity with each other, clearly indicating that Pd decoration does not influence the crystalline/structural properties of the native compound regardless of the concentration.

FE-SEM was employed to study the surface morphological features of the synthesized LSC and Pd-LSC composites, as illustrated in Fig. 2 with the corresponding TEM images. Bare LSC (Fig. 2a and b) shows the formation of grainy surface features

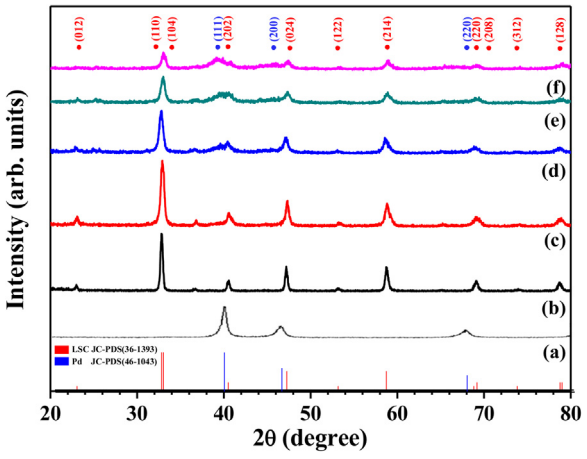

Fig. 1. XRD patterns of $La_{0.6}Sr_{0.4}CoO_{3-\delta}$ (LSC) perovskites: (a) Pd, (b) LSC, and (c) 5 wt.%, (d) 10 wt.%, (e) 20 wt.%, and (f) 30 wt.% Pd-LSC.

with porous nature, whereas, the deposition of Pd nanoparticles via the $NaBH_4$ reduction process induces the notable morphological change. More specifically, the transition from smooth morphology to the wrinkled cloth-like three-dimensional structure is evidence of the relatively uniform distribution of nanoscopic Pd particulates, with sizes of 5–8 nm. With the increase in Pd loading from 5 to 10 wt.% (Fig. 2), the Pd-LSC composite exhibited aggregation of the Pd particles over the three-dimensional structures observed at 5 wt.% loading. Further increase in the Pd concentration (Fig. 2) led to increased Pd particle density, i.e., severe aggregation and distortion of the Pd-LSC composite with more porosity. More specifically, for 20 and 30 wt.% Pd deposition (Fig. 2), the LSC surface seemed to be covered entirely with dense porous Pd particles, and distorted.

To clearly distinguish the structure and surface morphology of the Pd-LSC samples with various loadings, Cs-corrected TEM (Cs-TEM) measurements were performed and are presented in Fig. 3. Here, the Cs-TEM images of LSC and Pd-LSC surfaces are shown with the corresponding fast Fourier transform (FFT) and high-resolution TEM (HR-TEM) images in the inset. The Cs-TEM image of LSC (Fig. 3a) exhibits a plain smooth surface with a high degree of crystallinity. The d-spacing of 0.28 nm corresponds to the (110) plane of LSC, confirming the formation of high-quality LSC (JCPDS 36–1393). The Cs-Tem images of the Pd-LSCs with various loadings of nanoscopic Pd are given in Fig. 3b–e, which clearly indicate and ensure the deposition of Pd with the discernible difference in the individual morphology depending on the wt.% of Pd. In detail, the 5 wt.% Pd-LSC (Fig. 3b) shows some random distribution/deposition on the LSC surface. As the Pd loading increased from 5 to 10, 20, and 30 wt.%, the density of deposition also appeared to increase accordingly. Finally, the 30 wt.% Pd-LSC (Fig. 3e) exhibits higher Pd density, similar to the observation made by FE-SEM (Fig. 2e). The FFT and HR-TEM images in the insets of Fig. 3b–e could explain the deposition of Pd in detail with crystallographic lattice spacing. Fig. 3b–e clearly exhibit the lattice spacing of 0.23 nm for Pd-LSC that corresponds to 0.224 nm of Pd (JCPDS No. 46-1043). This d-spacing is consistent with the XRD observations.

The surface chemical composition of the synthesized Pd-LSC composites was analyzed through XPS, the results of which are given in Fig. 4. From the XPS, the main peaks, confirmed to be located at 834.2 and 837.2 eV, can be assigned to La $3d_{5/2}$ and La $3d_{3/2}$, respectively (Fig. 4). The peaks at 780.3, 528–531.5, and 133.2–135 eV, correspond to Co 2p, O 1s, and Sr $3d_5$, respectively [13,32]. The XPS survey spectra of the Pd-LSC samples with 5, 10, 20, and 30 wt.% loading of Pd exhibit characteristic Pd peaks in addition to the LSC energies. The binding energies of 335.2 and 340.5 eV could be assigned to Pd $3d_{5/2}$ and Pd $3d_{3/2}$, while the weak peaks at 336.8 and 343.2 eV are indicative of the presence of unreduced Pd^{2+}, as observed in Fig. 4. The main peak of La $3d_{5/2}$ shows two peaks located at 834.2 eV and 837.8 eV, which can be assigned to La $3d_{5/2}$ and La $3d_{3/2}$, respectively [33]. The small variations in the binding energy of the La $3d_{5/2}$ peaks and the spin-orbit splitting clearly suggest the presence of La atoms in 3^+ state [34]. The existence of two distinct peaks correspond to the 5/2 and 3/2 doublets, which are commonly found in complex oxides containing Sr. Apparently, the doublet separation (1.7 eV) and the binding energy of Sr are similar to those of Sr in SrO. The main peak appearing at 133.2 eV indicates the Sr^{2+} state and the peak shoulder appearing at 135 eV is due to $3d_{3/2}$ [35–37]. As Pd was deposited, the low energy peaks of Sr 3d in Pd-LSC gradually disappeared. The appearance of such high and low energy peaks is from the lattice and surface bound features of Sr. Similarly, the characteristic Co $2p_{3/2}$ peak was found at 780.3 eV, and the $2p_{1/2}$ peak position separated with the energy of 15 eV (795 eV), indicating spin-orbit splitting. This further confirms the presence of the characteristic Co^{2+} and Co^{3+} ions [32]. Moreover, the relative

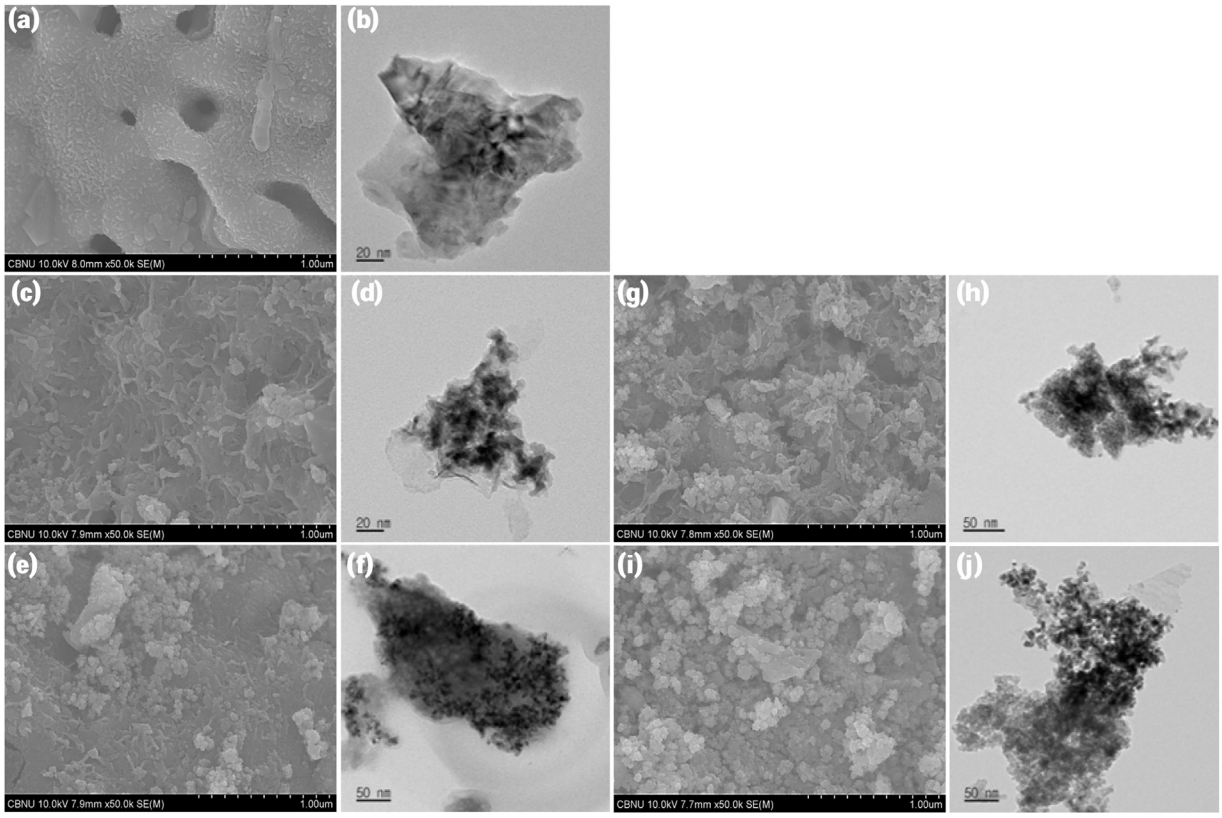

Fig. 2. FE-SEM and TEM images of LSC perovskites: (a, b) LSC, and (c, d) 5 wt.%, (e, f) 10 wt.%, (g, h) 20 wt.%, and (i, j) 30 wt.% Pd-LSC.

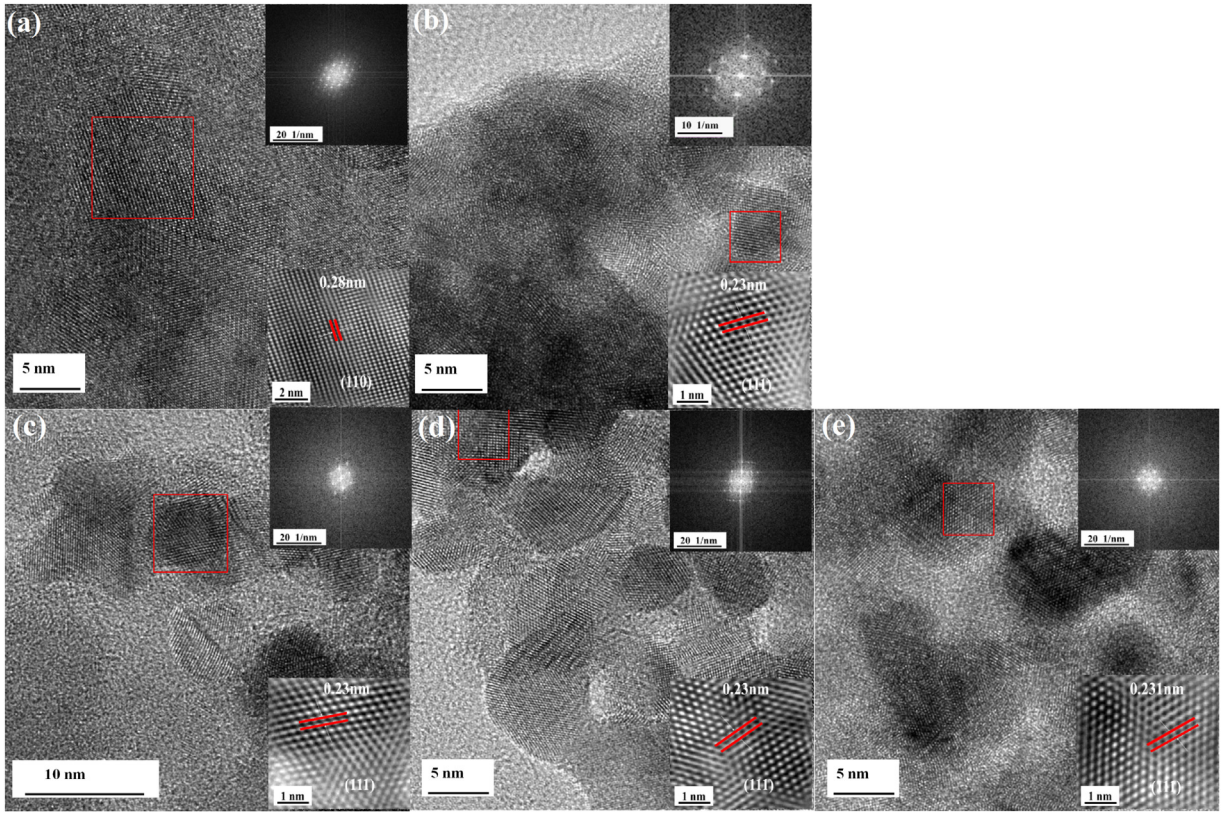

Fig. 3. HR-TEM images of LSC perovskites: (a) LSC, and (b) 5 wt.%, (c) 10 wt.%, (d) 20 wt.%, and (e) 30 wt.% Pd-LSC. The corresponding FFT images are given in the insets.

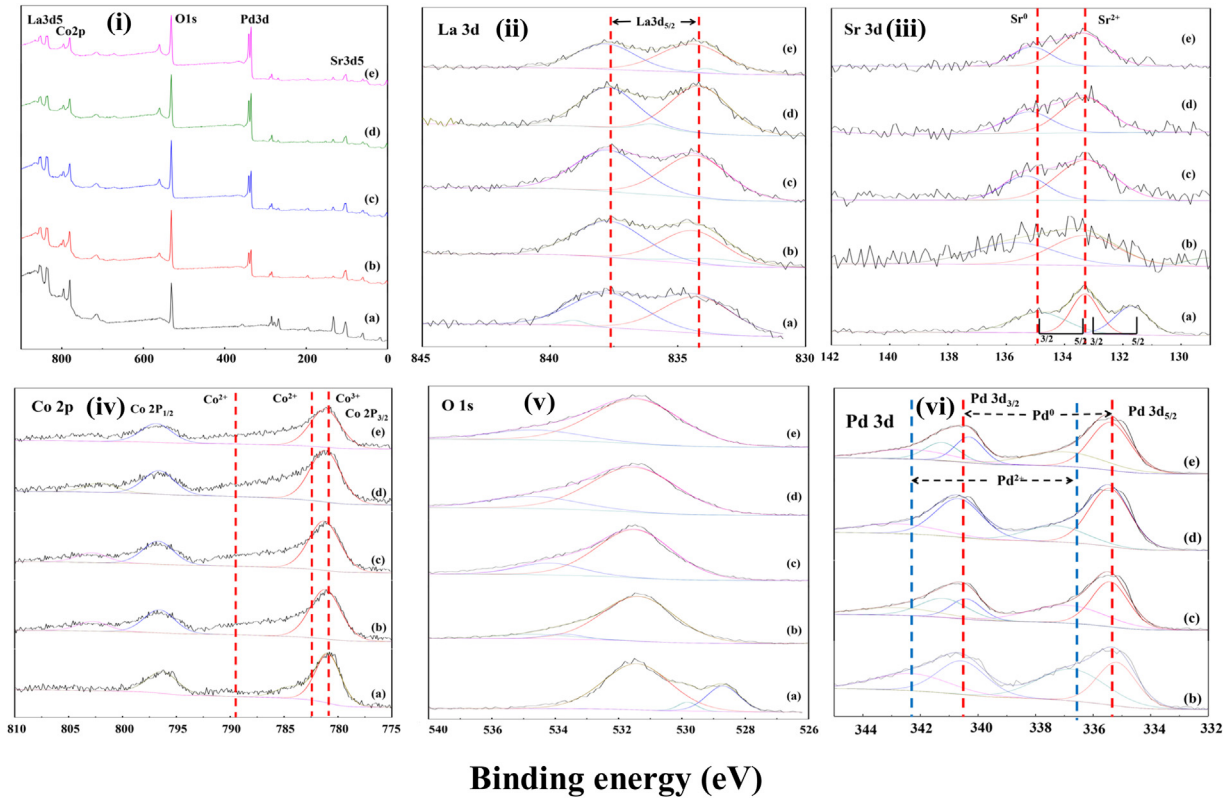

Fig. 4. Detailed XPS surveys of LSC perovskites with and without Pd-deposition: (a) LSC, and (b) 5 wt.%, (c) 10 wt.%, (d) 20 wt.%, and (e) 30 wt.% Pd-LSC.

intensity of and area below the main $2p_{3/2}$ line suggest the dominant presence of Co^{3+} (approximately 2 for Co^{3+}/Co^{2+}). The O 1s spectra measured at 529–530.1 eV is of the surface-oxygen species (M (Sr, La, Co)-O), while the highest energy (531–531.5 eV) occurred due to the influence of the surface oxygen-functionalities present in the compounds. The Pd peak appears as a Pd $3d_{5/2}$ and Pd $3d_{3/2}$ doublet signal at 335.2 and 340.5 eV, respectively [38]. It is well known that XPS is only suitable for surface analysis, however, the bulk analysis is much more important. Hence, the chemical compositions were estimated through ICP-MS and are given in Table 1, in which both theoretical and experimental analyses of the LSC samples were conducted. It should be noted that the calculated and measured values coincide very well, indicating the proper synthesis and appropriate composition of the Pd-LSC samples with the anticipated proportions.

The N_2 adsorption and desorption properties of the synthesized materials were studied via BET measurements, as shown in Fig. 5, along with the physical properties, i.e., specific surface area, pore volume, and mean pore diameter. As can be seen in Fig. 5, type IV isotherm is shown for the Pd-LSC materials, indicating the mesoporous nature of the prepared composites [39]. Increase of the hysteresis suggests further uptake of N_2 due to increases in the surface area and porosity. Accordingly, the specific surface area dramatically increased from 0.2 $m^2\,g^{-1}$ to 21.11 $m^2\,g^{-1}$ when the loading was increased from 0 to 20 wt.%. However, a small deviation was observed (20.94 $m^2\,g^{-1}$) for the case of 30 wt.% loading; although this deviation is highly negligible, it is a better result than of the native compound, LSC. Generally, the Pd particles tended to aggregate upon high concentration, which could explain the marginal deviation of the specific surface area.

Table 1
ICP–MS analysis of LSC and Pd-deposited LSC.

ICP-MS								
	La%		Sr%		Co%		Pd%	
Sample	n	e	n	e	n	e	n	e
LSC	36.9	34	15.5	16	26.1	27	–	–
5 wt.% Pd-LSC	35.1	34	14.7	13	24.8	27	5	5
10 wt.% Pd-LSC	33.3	33	14	12	23.5	22	10	10
20 wt.% Pd-LSC	29.5	29	12.4	10	20.9	20	20	19
30 wt.% Pd-LSC	25.8	25	10.8	9	18.3	17	30	30

*n = nominal value, e = experimental value.

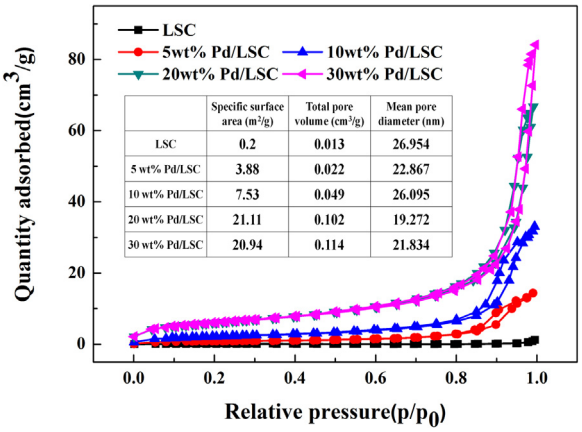

Fig. 5. N_2 adsorption/desorption isotherm of LSC and Pd-deposited LSC; The inset table presents the quantitative surface properties, i.e., surface area, pore volume, and mean pore diameter, of the synthesized materials, as deduced from Fig. 5.

Electrochemical characteristics in the aqueous medium

LSV was employed to study the electrocatalytic activity, i.e., ORR and OER, of the synthesized Pd-LSC composites, as shown in Fig. 6. The electrocatalytic activity of the commercial Pt/C, RuO_2,

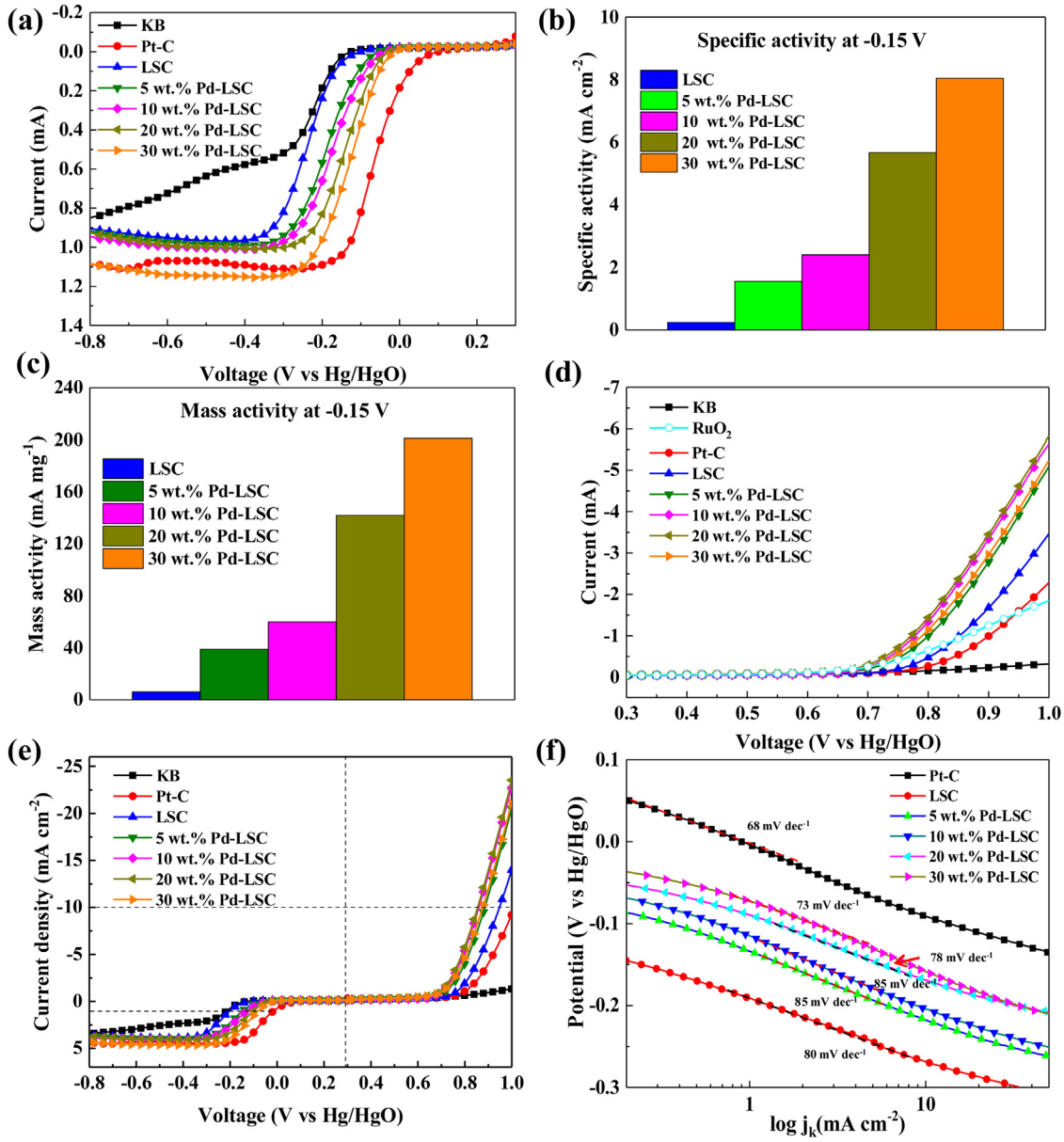

Fig. 6. (a) ORR polarization curves, (b) specific activity at –0.15 V, (c) mass activity at –0.15 V, (d) OER polarization curves, (e) potential difference between the ORR and OER curves, and (f) Tafel plots of LSC, Pd-LSC, KB, and Pt measured in O_2-saturated 0.1 M KOH solution at 5 mV s^{-1}.

and KB samples were also measured under the same experimental conditions for comparison. In the ORR measurements, it is obvious that the native LSC requires a relatively higher onset potential (–0.158 V) compared to its Pd-decorated composites. However, the LSC holds better onset potential than the KB; whereas, all the Pd-LSC composites exhibit much lower onset potential than the native compound. Interestingly, the ORR activity of LSC increases according to the Pd loading in the composite. Amongst the composites, 30 wt.% Pd loading displayed superior ORR activity with high limiting current (1.09 mA) and required lower onset potential (–0.030 V), quite comparable to that of the commercial Pt/C catalyst. This implies that Pd plays an important role in enhancing the ORR activity of LSC, which is clearly validated through ORR traces. Pd catalytic activity toward the ORR is generally known to be much lower than that of Pt or its alloys [40]. However, in this work, we demonstrate that Pd decoration on LSC also renders significant enhancement in the ORR activity. The structural analytical study of the synthesized Pd-LSC composites shows that with increasing Pd wt.%, the LSC surface became completely covered with dense porous Pd particles (Figs. 2 and 3), increasing the specific surface area (Fig. 5). Previously [28,29,41], it was suggested that the ORR activity of perovskite catalysts (e.g., LSC) can be improved by tailoring the morphological aspect, for example, increasing the specific surface area, besides making the carbonaceous composites. All the measured ORR values, like the onset potential and limiting current, for all the samples are presented in Table S2 for easier comparison. Furthermore, a quantitative estimation of the activity of the catalysts subjected for ORR was calculated from the ORR curves at –0.1, –0.15, and –0.2 V vs. Hg/HgO, as in Figs. 6b and c for –0.15 V only. The Pd-LSC perovskites displayed higher mass and specific activities than the native LSC and commercial KB. As expected, both the mass and specific activities correlate with the increasing Pd content in the Pd-LSC composite, which signifies the importance of Pd decoration of the composite toward promoting the catalytic activity. As discussed, the ORR activity increased proportionally to Pd loading

via the increase in specific surface area and porosity. Additionally, the participation of the Pd nanoparticles in the catalytic activity is worth mentioning. In our previous work [28,29], we studied the influence of a specific surface area of LSC using ball milling toward ORR activity, but the incremental activity was found to be minimal compared to the present work. The utilization of Pd deposition is vital to significantly increase the ORR activity in two ways: (i) increasing the active surface by pore formation, and (ii) participating in the electrochemical reaction. Hence, it is evident that Pd plays a major role in the enhancement of the ORR activity by increasing the active surface area and is highly comparable to that of the commercially available well-known catalyst, Pt/C.

Similar to the ORR activity, the OER characteristics were also recorded for all the samples, including RuO_2, KB, and Pt/C, and are presented in Fig. 6d. As previously mentioned, and well-established, perovskite-type LSC is an excellent catalyst for OER activity [21,24]. In contrast to ORR activity, the native LSC displayed better OER activity than those of commercial RuO_2, KB, and Pt/C. The introduction of Pd decoration on the LSC surface results in a decrease in the onset potential for the OER performance. Furthermore, OER activity has a nonlinear relationship with Pd loading. For example, the 20 wt.% Pd-decorated LSC exhibited better activity than the 30 wt.% Pd-decorated LSC, which is in contrast to the ORR studies. This deviation in the linear variation clearly indicates that the higher specific surface area and higher amount of Pd decoration do not decisively affect the OER activity. Hence, to improve the OER activity, optimal specific surface area and loading are necessary to yield a better performing catalyst. Moreover, there is no direct relationship between electrocatalytic activity and Pd concentration. In previous studies, it has also been reported that the OER catalytic activity of Pd could be significantly improved by making alloys with metastatic metals, such as Co, Ni, Cr, and Fe [42], or by the distribution of various nanostructured metal oxides on the surface [43,44].

Generally, the bifunctional electrocatalytic behavior of any catalyst can be assessed by measuring the potential difference between the ORR and OER activity (Fig. 6e), as presented in Table S2. More specifically, the 30 and 20 wt.% Pd loadings displayed better ORR and OER activities in an aqueous medium, respectively. The catalyst must hence be chosen with the minimum potential difference between the ORR and OER activities. Accordingly, the potentials of the ORR curves were selected at the current density of 1 mA cm^{-2}, which is almost half-wave potential. In the case of OER, we chose the current density necessary for the oxidation of water, i.e., fixed at 10 mA cm^{-2}, as it is a widely accepted range [45,46]. It is clear that all Pd-decorated LSC exhibited lower oxygen electrode potential than LSC, regardless of the concentration, and the oxygen electrode potential linearly varied, i.e., decreased, indicating the increase of bifunctional electrocatalytic activity. Accordingly, the 30 wt.% Pd loading displayed the lowest oxygen electrode potential difference (0.945 V) compared to the other compositions investigated. It is interesting to note that the 30 wt.% Pd-LSC exhibited a much lower potential difference than commercially available Pt/C (1.025 V). Furthermore, it is well known that the oxygen reactions at the surface of the perovskite catalyst take place through very complex reaction steps, such as oxygen adsorption-dissociation, oxygen surface diffusion, and oxygen bulk diffusion [47]. A noble metal decoration of perovskite catalysts greatly improves the bifunctional catalytic activity of the perovskite oxides as the noble metals promote oxygen reactions (ORR and OER) by activating oxygen adsorption-dissociation and diffusions. Similar observations have also been made previously in various catalytic reactions [48,49]. The studies have shown that the perovskite catalytic reactivity could be greatly enhanced by decorating metal or metal oxide on the surface.

Fig. 6f shows the Tafel plots of the Pd-LSC samples together with native LSC, Pt/C, and KB for comparison. The Tafel plots were obtained by plotting the logarithm of the kinetic current density derived from the ORR curves given in Fig. 6a. The kinetic current density (j_k) was calculated by the equation below.

Here j and j_d represent the limiting current density and disk current density, respectively, which can be measured from the ORR traces. The 30 wt.% Pd-LSC composite exhibits a slope of 73 mV dec^{-1}, which is the closest value to the commercial Pt/C (68 mV dec^{-1}) catalyst. A comparison of the Tafel slopes clearly suggests that the 30 wt.% Pd-decorated LSC sample could be a promising candidate for use as a catalyst, following a similar catalytic reaction mechanism as that of Pt/C during ORR activity [50]. Furthermore, it is inferred that the catalytic activity is directly related to the specific surface area and porous structure. However, the medium of reaction is also important as it determines the usefulness of the catalyst prepared for potential applications. Interestingly, the ORR and OER activities, mechanism, and performance may not be the same for aqueous and organic media. However, some catalysts are found to be exceptional, for instance, Pd, Pt, Ru, Au, and GC are capable of displaying improved catalytic activity in both organic and aqueous solutions. Regarding the present study, the catalytic activity of Pd-decorated LSC in an organic medium is yet to be studied, to explore its potential use as a catalyst in Li-O_2 batteries. More specifically, Pd is well known for its catalytic activity, which catalyzes four electron transfer, as reported by Lu et al. [51] and others [52,53]. Lu et al. [51] studied the ORR activity of the aforementioned precious metal catalysts toward Li-O_2 batteries and found the ORR activity to be in the order of Pd > Pt > Ru ≈ Au > GC on bulk surfaces in non-aqueous medium. The intrinsic Li^+-ORR activities of the five surfaces (Pd, Pt, Ru, Au, and GC) showed a volcano shape as a function of the oxygen adsorption energy relative to that of Pt (per oxygen atom relative to an atom in the gas phase); for example, the ORR activity increased from GC to Au, trailed by Pt, and peaked at Pd as the oxygen adsorption energy increased. The further increase resulted in a decrease in the activity of Ru compared to Pd, positioned at the peak forming a typical "volcano-type" relationship. This volcano formation depends on the strength of oxygen binding on the catalyst surface [51–53]. In the same way, we anticipated the catalytic activity of the Pd-LSC composite toward Li-O_2 battery application.

Electrochemical characteristics in the organic medium

To ensure catalytic activity in an organic medium (1 M LiTFSI in TEGDME), the Pd-LSC composites were tested via CV for Li-O_2 battery application potential. For the CV studies, the best-performing composition in the aqueous medium was chosen (30 wt.% Pd-LSC); the native LSC and KB electrodes were also compared under the same experimental conditions. The CV studies were conducted for a wide potential range of 1.5–4.7 V vs. Li at a scan rate of 0.01 mV s^{-1}, as shown in Fig. 7a. All the three samples exhibited very sharp reduction potentials, of 2.49, 2.53, and 2.56 V vs. Li for KB, LSC, and 30 wt.% Pd-LSC, respectively. This reduction reaction of oxygen can be written as $Li^+ + O_2 \rightarrow 2e- + Li_2O_2$ [50,54]. During oxidation, prominent and high-intensity peaks, observed at 4.25, 4.43, and 4.54 V vs. Li, were noted for 30 wt.% Pd-LSC, LSC, and KB, respectively [54,55]. The existence of very tiny peaks for the 30 wt.% Pd-LSC sample at 3.2 and 3.4 V vs. Li are due to the formation of intermediates like Li-O_2 upon the oxidation of O_2 during the charge process [54,55]. The peak current for the reduction reaction is more prominent and higher than that of the evolution reaction owing to the sluggish kinetics and because of these multiple oxidation peaks. It is interesting that the observed variation during the Li_2O_2 formation and decomposition, i.e.,

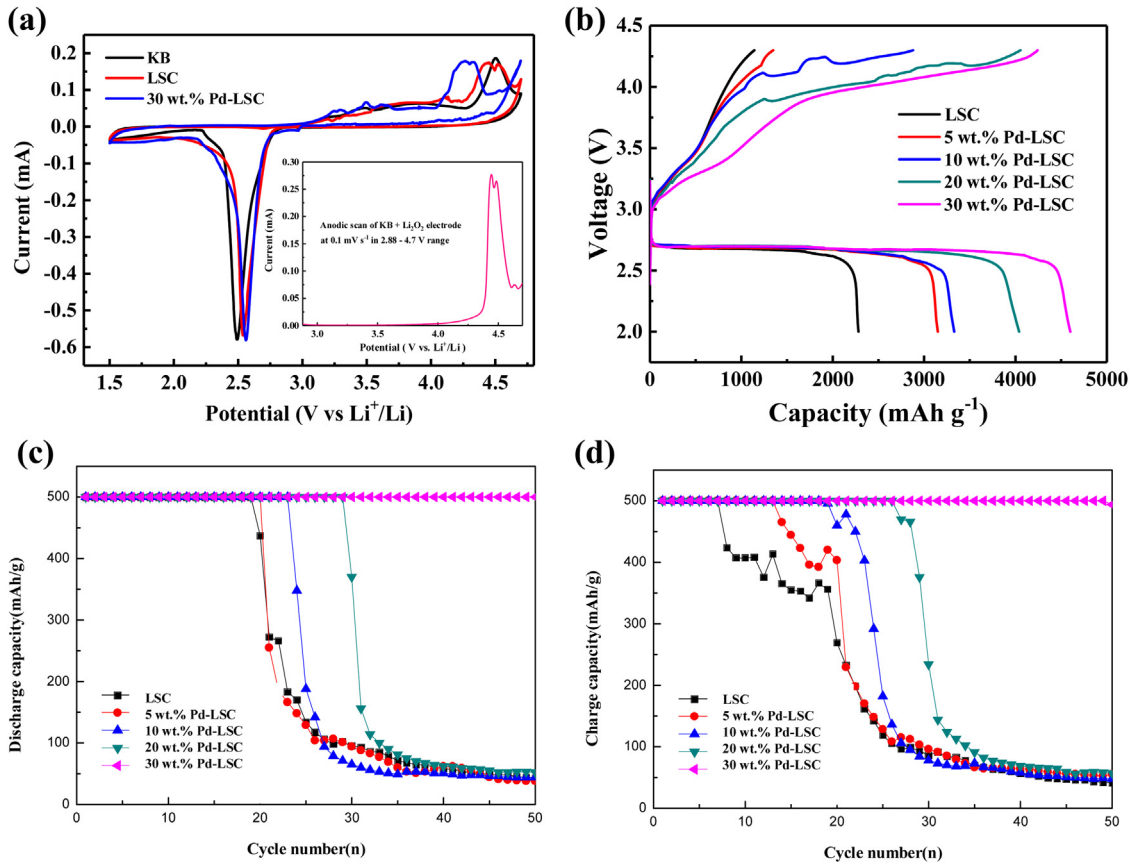

Fig. 7. (a) Cyclic voltammograms of the cathodes with and without Pd deposition in 1 M LiTFSI (TEGDME) electrolyte at a scan rate of 0.01 mV s^{-1} over a potential range of 1.5–4.7 V at room temperature under O_2 atmosphere; (b) First charge–discharge profiles; (c, d) Cycle life efficiency of the Li-O_2 battery using LSC perovskite catalysts with and without Pd deposition ((c) discharge and (d) charge).

organic medium, is consistent with that observed in the aqueous medium. This CV study not only validates that the 30 wt.% Pd-LSC could be used as an efficient catalyst for effective ORR and OER, but also proves activity in organic medium with less polarization, compared to the KB and native LSC. Furthermore, to ensure the possibility of their use in Li-O_2 batteries, the Swagelok^{TM}-type test cell was used and subjected to a galvanostatic analysis. This will be discussed in the forthcoming Section.

Lithium-O_2 battery applications

Galvanostatic charge–discharge studies were conducted for all the Pd-decorated samples, including native LSC, at a current density of 0.1 mA cm^{-2}, as shown in Fig. 7b. The Li-O_2 cell delivered the first discharge capacities of 2150, 3150, 3330, 4055, and 4601 mA h g^{-1} for 0, 5, 10, 20, and 30 wt.% Pd loading on the LSC, respectively. The 30 wt.% Pd-deposited LSC delivered the maximum discharge capacity of 4601 mA h g^{-1}. In addition to this higher capacity, the over-potential was found to be minimum for the case of 30 wt.% Pd loading; 1.32, 1.27, 1.0, and 0.8 V were observed for 5, 10, 20, and 30 wt.% Pd loading, respectively. The coulombic efficiency is another crucial factor for the efficient operation of the cell. The coulombic efficiency can be calculated from the 100% ratio of the charge and discharge capacities obtained in Fig. 7b. The efficiency was low, at around 50% for LSC and 5% for Pd-LSC, but was relatively high for 10–30 wt.% Pd-LSC. Correspondingly, the 20 wt.% Pd-LSC samples displayed marginally improved reversibility (100%) than the 30 wt.% Pd-LSC catalyst (92.2%). The increase in the efficiency of Li-O_2 batteries correlates with the increase in charge capacity, which means that the Li_2O_2 solid oxides produced during the discharge process break down well and are easily removed from the electrode surface. More specifically, the increase in efficiency indicates that the activity of the catalyst used is high, making it easier to remove Li_2O_2. These results are consistent with those of the OER (Fig. 6d), which presents maximum activity for 20 wt.% Pd-LSC. Overall, the decoration of high Pd content over LSC is beneficial to the Li-storage process in terms of high capacity, reversibility, and lower overpotential compared to the other compositions examined. It is clear that the synergistic effect of Pd decoration over LSC certainly promoted the reduction and oxidation reactions at the air cathode, and eventually improved the Li-O_2 battery

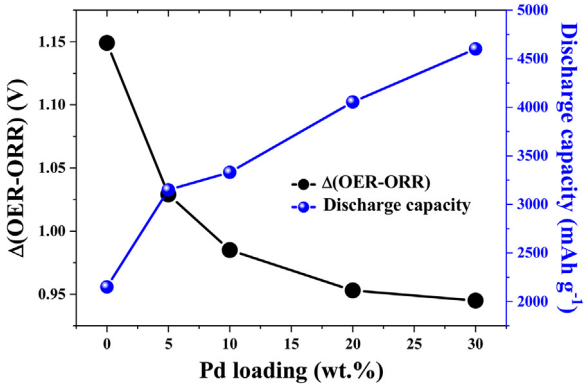

Fig. 8. Electrochemical and battery performance characterizations as a function of Pd wt.%.

performance. The cycling profiles of the Li-O_2 batteries were obtained with the capacity limit of 500 mA h g^{-1} for both charge and discharge at the constant current density of 0.1 mA cm^{-2}, as shown in Figs. 7c and d. As expected, the 30 wt.% Pd-decorated LSC air cathodes rendered very stable cycling behavior compared to the other loadings of LSC. Interestingly, the increase in Pd loading improved the electrochemical behavior of the Li-O_2 battery (Fig. S1). Fig. 8 concisely summarizes the electrochemical and battery performance characterizations of the Pd-decorated LSC catalyst. Increasing the Pd wt.% in the Pd-LSC composite led to a decrease in the overpotential of the Li-O_2 battery with an increase in the discharge capacity.

Post-characterization

A postmortem analysis is crucial to understand the charge-storage process, particularly during the formation and decomposition of Li_2O_2. Hence, the surface morphological features and composition of the air electrodes were investigated through XRD (Figure S2) and FE-SEM, as displayed in Fig. 9. The XRD patterns were also recorded prior to the charge–discharge process for comparison, in which characteristic reflections of inactive materials, like carbon ($2\theta = 23^\circ$ and 44°), TAB ($2\theta = 17^\circ$), and Ni ($2\theta = 43.5^\circ$, 47.6°, and 51°) peaks, were observed from all samples [56]. For the case of LSC, after the first discharge, the XRD peaks show the

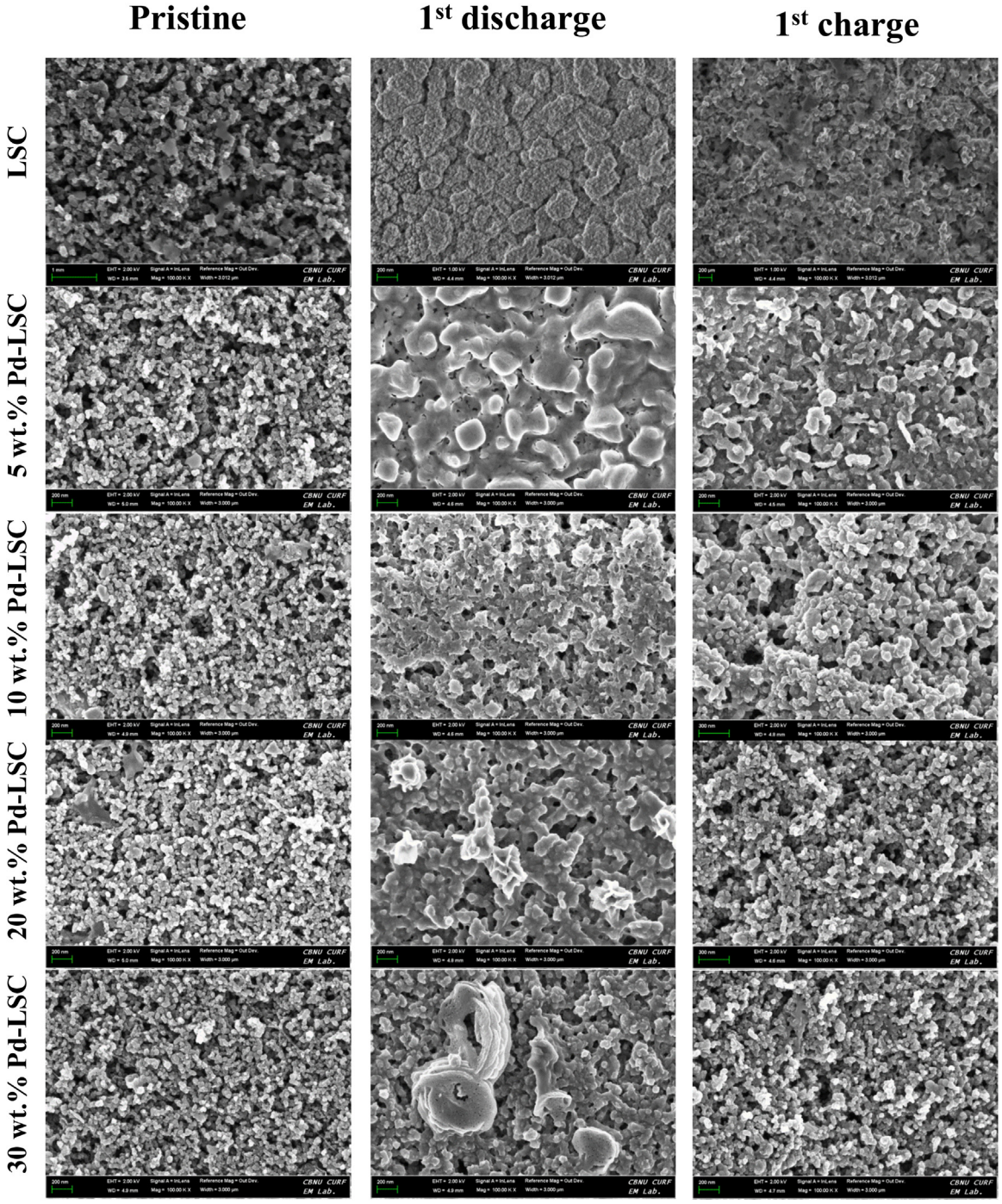

Fig. 9. FE-SEM images before and after discharge/charge during the first cycle for air cathodes.

formation of Li_2O_2 at $2\theta = 32^\circ$, 35°, and 58° as a discharge product, which remained on the electrode surface even after the charging process, suggesting poor decomposition [56,57]. The XRD patterns of the Pd-decorated LSC catalyzed cathodes clearly indicate the formation and decomposition of Li_2O_2. The intensity of the Li_2O_2 peak position is very weak, hence, it is difficult to see as prominent. To supplement the aforementioned reaction, the FE-SEM studies were conducted, as in Fig. 9. All the samples exhibited very smooth surface morphologies prior to the electrochemical studies. Completely different surface morphological features were seen from the air cathode with prominent agglomerations after discharge. This agglomeration clearly suggests the formation of Li_2O_2. Upon charging, the agglomeration remained on the native LSC electrode, indicating the poor decomposition of Li_2O_2. Moreover, the Pd-decorated LSC catalyzed electrodes that exhibited scattered agglomerations over the surface, i.e., 5 and 10 wt.%, suggest the incomplete decomposition of Li_2O_2. Meanwhile, the rate of decomposition is far better than that of the native LSC. In the case of 30 wt.% Pd-deposited LSC, almost the same morphology was exhibited, which was seen prior to the electrochemical studies. This is very similar to the results observed for the coulombic efficiency. The efficiency increased as the content of Pd increased and showed high values over 90% for 20 and 30 wt.% Pd-LSC, indicating the disappearance of Li_2O_2 aggregation from the electrode surface. This proves that 30 wt.% Pd-deposited LSC is an efficient catalyst for the decomposition of the solid discharge product, Li_2O_2, which corresponds to the electrocatalytic activity in an aqueous medium. More specifically, this Pd-decorated LSC can be used as an efficient catalyst regardless of the working medium, i.e., aqueous or organic. Further studies are in progress to improve the limiting capacity of the Li-O_2 cell to 1000 mA h g^{-1}.

Conclusions

We successfully demonstrated the decoration of nanoscopic Pd over perovskite LSC surface to improve the catalytic efficiency for Li-O_2 battery application by increasing the ORR activity. The decoration of higher Pd wt.% on the LSC surface not only increases the specific surface area, but also improves the porous nature of the catalyst. The highly concentrated (e.g., 30 wt.%) Pd-LSC catalyst rendered better catalytic activity than the native compound and is comparable to the commercially available Pt/C catalyst through studies of the ORR and OER activities in an aqueous medium. The catalytic behavior of Pd-LSC was found to have a linear relationship with the Pd loading for ORR activity, whereas, nonlinear behavior was observed for OER activity. Similar to the aqueous media, the 30 wt.% Pd-decorated LSC sample displayed better behavior in the air electrode in terms of less overpotential, high capacity, and stable cycling profile in terms of Li-O_2 battery application. The present study clearly suggests that Pd decoration over LSC could be used as an efficient catalyst regardless of the medium, and more specifically to improve the Li-O_2 battery performance by increasing the ORR catalytic activity for an oxygen electrode catalyst toward building the next generation of high-energy density power packs.

Acknowledgments

This paper was supported by Post-Retired Research Professor research funds of Chonbuk National University in 2017.

Appendix A. Supplementary data

Supplementary material related to this article can be found, in the online version, at doi:https://doi.org/10.1016/j.jiec.2019.08.045.

References

[1] T. Ogasawara, A. Débart, M. Holzapfel, P. Novák, P.G. Bruce, J. Am. Chem. Soc. 128 (2006) 1390.
[2] P.G. Bruce, S.A. Freunberger, L.J. Hardwick, J.-M. Tarascon, Nat. Mater. 11 (2012) 19.
[3] P.G. Bruce, Solid State Ionics 179 (2008) 752.
[4] Z. Peng, S.A. Freunberger, Y. Chen, P.G. Bruce, Science 337 (2012) 563.
[5] J. Lu, L. Li, J.-B. Park, Y.-K. Sun, F. Wu, K. Amine, Chem. Rev. 114 (2014) 5611.
[6] P. Sennu, M. Christy, V. Aravindan, Y.-G. Lee, K.S. Nahm, Y.-S. Lee, Chem. Mater. 27 (2015) 5726.
[7] P. Sennu, H.S. Park, K.U. Park, V. Aravindan, K.S. Nahm, Y.-S. Lee, J. Catal. 349 (2017) 175.
[8] A. Débart, A.J. Paterson, J. Bao, P.G. Bruce, Angew. Chem. Int. Ed. 47 (2008) 4521.
[9] N. Ominde, N. Bartlett, X.-Q. Yang, D. Qu, J. Power Sources 185 (2008) 747.
[10] C. Tran, J. Kafle, X.-Q. Yang, D. Qu, Carbon 49 (2011) 1266.
[11] T. Zhang, N. Imanishi, Y. Shimonishi, A. Hirano, Y. Takeda, O. Yamamoto, N. Sammes, Chem. Commun. 49 (2010) 1661.
[12] J. Suntivich, H.A. Gasteiger, N. Yabuuchi, H. Nakanishi, J.B. Goodenough, Y. Shao-Horn, Nat. Chem. 9 (2011) 546.
[13] P. Sennu, V. Aravindan, K.S. Nahm, Y.-S. Lee, J. Mater. Chem. A 5 (2017) 18029.
[14] W. Yang, J. Salim, S. Li, C. Sun, L. Chen, J.B. Goodenough, Y. Kim, J. Mater. Chem. 22 (2012) 18902.
[15] X. Xu, W. Wang, W. Zhou, Z. Shao, Small Methods 2 (2018) 1800071.
[16] X. Xu, Y. Chen, W. Zhou, Y. Zhong, D. Guan, Z. Shao, Adv. Mater. Interfaces 5 (2018) 1701693.
[17] X. Xu, C. Su, W. Zhou, Y. Zhu, Y. Chen, Z. Shao, Adv. Sci. 3 (2016) 1500187.
[18] P. Tan, M. Liu, Z. Shao, M. Ni, Ad. Energy Mater. 7 (2017) 1602674.
[19] Z. Wang, Q. Li, Y. Chen, B. Cui, Y. Li, F. Besenbacher, M. Dong, NPG Asia Mater. 10 (2018) 703.
[20] Z. Wang, H.-H. Wu, Q. Li, F. Besenbacher, X.C. Zeng, M. Dong, Nanoscale 10 (2018) 18178.
[21] Y. Zhao, L. Xu, L. Mai, C. Han, Q. An, X. Xu, X. Liu, Q. Zhang, Proc. Natl. Acad. Sci. U.S.A 109 (2012) 19569.
[22] N. Sun, H. Liu, Z. Yu, Z. Zheng, C. Shao, Solid State Ionics 268 (2014) 125.
[23] F. Lu, Y. Wang, C. Jin, F. Li, R. Yang, F. Chen, J. Power Sources 293 (2015) 726.
[24] J. Suntivich, K.J. May, H.A. Gasteiger, J.B. Goodenough, Y. Shao-Horn, Science 334 (2011) 1383.
[25] J. Zhang, Y. Zhao, X. Zhao, Z. Liu, W. Chen, Sci. Rep. 4 (2014)6005.
[26] Z. Du, P. Yang, L. Wang, Y. Lu, J.B. Goodenough, J. Zhang, D. Zhang, J. Power Sources 265 (2014) 91.
[27] Y. Wu, T. Wang, Y. Zhang, S. Xin, X. He, D. Zhang, J. Shui, Sci. Rep. 6 (2016)24314.
[28] M.Y. Oh, J.S. Jeon, J.J. Lee, P. Kim, K.S. Nahm, RSC Adv. 5 (2015) 19190.
[29] J.J. Lee, M.Y. Oh, K.S. Nahm, J. Electrochem. Soc. 163 (2016) A244.
[30] E. Antolini, Energy Environ. Sci. 2 (2009) 915.
[31] J. Shi, X. Hu, J. Zhang, W. Tang, H. Li, X. Shen, N. Saito, Prog. Nat. Sci.: Mater. Int. 24 (2014) 593.
[32] D.H. Prasad, S.Y. Park, E.O. Oh, H. Ji, H.R. Kim, K.J. Yoon, J.W. Son, J.H. Lee, Appl. Catal. A: Gen. 447 (2012) 100.
[33] E.Y. Konysheva, S.M. Francis, J.T.S. Irvine, A. Rolle, R.-N. Vannier, J. Mater. Chem. 21 (2011) 15511.
[34] P. Wang, L. Yao, M. Wang, W. Wu, J. Alloys Compd. 311 (2000) 53.
[35] K. Tabata, I. Matsumoto, S. Kohiki, J. Mater. Sci. 22 (1987) 1882.
[36] N. Gunasekaran, N. Bakshi, C.B. Alcock, J.J. Carberry, Solid State Ionics 22 (1996) 145.
[37] E.J. Crumlin, E. Mutoro, Z. Liu, M.E. Grass, M.D. Biegalski, Y.-L. Lee, D. Morgan, H. M. Christen, H. Bluhm, Y. Shao-Horn, Energy Environ. Sci. 5 (2012) 6081.
[38] J.M. Giraudon, A. Elhachimi, G. Leclercq, Appl. Catal. B: Environ. 84 (2008) 251.
[39] H.-Q. Dong, Y.-Y. Chen, M. Han, S.-L. Li, J. Zhang, J.-S. Li, Y.-Q. Lan, Z.-H. Dai, J.-C. Bao, J. Mater. Chem. A 2 (2014) 1272.
[40] R. Pattabiraman, Appl. Catal. A: Gen. 153 (1997) 9.
[41] C. Jin, Z. Yang, X. Cao, F. Lu, R. Yang, Int. J. Hydrogen Energy 39 (2014) 2526.
[42] W. Wang, D. Zheng, C. Du, Z. Zou, X. Zhang, B. Xia, H. Yang, D.L. Akins, J. Power Sources 167 (2007) 243.
[43] Q. Qu, J.H. Zhang, J. Wang, Q. Yu Li, C.W. Xu, X. Lu, Sci. Rep. 7 (2017)41542.
[44] Z.Y. Li, Z.L. Liu, J.C. Liang, C.W. Xu, X. Lu, J. Mater. Chem. A 2 (2014) 18236.
[45] Y. Gorlin, T.F. Jaramillo, J. Am. Chem. Soc. 132 (2010) 13612.
[46] Y. Matsumoto, E. Sato, Mater. Chem. Phys. 14 (1986) 397.
[47] S. Guo, H. Wu, F. Puleo, L.F. Liotta, Catalysts 5 (2015) 366.
[48] Y. Gong, X. Zhang, Z. Li, Z. Wang, C. Sun, L. Chen, ChemNanoMat 8 (2017) 485.
[49] H. Jang, A. Zahoor, Y. Kim, M. Christy, M.Y. Oh, V. Aravind, Y.S. Lee, K.S. Nahm, Electrochim. Acta 212 (2016) 701.
[50] J. Du, Y. Pan, T. Zhang, X. Han, F. Cheng, J. Chen, J. Mater. Chem. 22 (2012) 15812.
[51] Y.-C. Lu, H.A. Gasteiger, Y. Shao-Horn, J. Am. Chem. Soc. 133 (2011) 19048.
[52] W. Sun, A. Hsu, R. Chen, J. Power Sources 196 (2011) 4491.
[53] K.-N. Jung, A. Riaz, S.-B. Lee, T.-H. Lim, S.-J. Park, R.-H. Song, S. Yoon, K.-H. Shin, J.-W. Lee, J. Power Sources 244 (2013) 328.
[54] C.O. Laoire, S. Mukerjee, K.M. Abraham, E.J. Plichta, M.A. Hendrickson, J. Phys. Chem. C 113 (2009) 20127.
[55] C.O. Laoire, S. Mukerjee, K.M. Abraham, E.J. Plichta, M.A. Hendrickson, J. Phys. Chem. C 114 (2010) 9178.
[56] H. Jang, A. Zahoor, J.S. Jeon, P. Kim, Y.S. Lee, K.S. Nahm, J. Electrochem. Soc. 162 (2015) A300.
[57] Y. Hu, X. Han, F. Cheng, Q. Zhao, Z. Hu, J. Chen, Nanoscale 6 (2014) 177.